Experimental investigation of solitary breaking waves in the swash zone

Lisa Smith[a], Atle Jensen[a], Geir Pedersen[a]

[a] Department of Mathematics, University of Oslo, Norway

Abstract

This study presents an experimental investigation of plunging breakers on a sloping beach with an inclination of 5.1°. The incident waves are solitary waves with various amplitudes from non-breaking waves to plunging breakers, and the area investigated is the swash zone. PIV (Particle Image Velocimetry) is performed on images captured at four different field of views (FOV). The PIV measurements are compared with computed velocity fields from a Boundary Integral Model (BIM). There is excellent agreement between the experimental and the computed result for the non-breaking waves. The experimental results from the breaking waves indicate that the motion becomes more irregular as we move further up the beach. In addition, there are more irregularities present for waves with larger amplitude. Shoreline position and maximum runup are measured, and are repeatable in both time and height, although cross-sectional variations of the shoreline shape are observed at maximum runup. Length and velocity of air bubbles entrapped by the plunger breakers are extracted from a image series captured with large a FOV. The images showed that a large air bubble remains intact for a time period during runup for the breaking waves.

Keywords:

1. Introduction

In shallow water with constant depth, the nonlinear effect and dispersion will be balanced for solitary waves [9]. If the depth decreases as the wave travels towards the shore, the wave will steepen, and at some critical point breaking may occur. Breaking waves are one of the most important physical features in the swash zone [4]. Breaking waves have a large impact on sediment transport onshore, which can result in erosion on cliffs and affect construction located near the shore. Although breaking waves is a well-known phenomenon from our daily life, many physical aspects regarding wave breaking are still poorly understood.

Several experimental studies of breaking waves have been performed in the recent years. A broad range of different experimental methods have been utilized to measure quantities such as surface elevation, runup, shear stress, and velocities. Techniques such as Laser Doppler Velocimetry [10], PIV [2] and shear sensors [1] has been utilized. The swash zone is defined as the region where the beach is partly wetted during runup and rundown. Aeration and the small flow depth makes the swash zone a challenging region to study experimentally with the techniques mentioned above. A further development of the PIV method is Bubble image Velocimetry (BIV), which [12] use to investigate velocity fields in plunging breakers. They compared

the measurements with numerical simulations conducted with Reynolds Average Navier Stokes Equations model. The model gave fairly good agreement with the measurements in the surf zone, but the model overpredicts the velocities in the swash zone compared to the BIV measurements. One of the latest work on solitary waves on a plane beach has been conducted by [11]. They investigated the flow evolution of the runup and run down of solitary waves in the range from non breaking to plunging breakers. A shear plate was located at different position along the beach and measurements revealed that the maximum positive bed shear stress was obtained in the tip if the swash tongue during runup, and is due to the developing of a boundary layer, and bore driven turbulence. The maximum negative bed shear stress was obtained at the end of the withdrawal. The flow is accelerated during downrush by gravity and the bed shear stress increases during rundown intil a maximum is reached right before the water runs out of the measuring area.

Until now, PIV measurements with high resolution close to the beach have not been reported for breaking waves in the swash zone. This paper presents PIV measurements where the amplitude of the solitary breaking waves varies. The paper starts with a description of the experimental set-up and the the Boundary Integral Model used in this study (chapter 2). Further on, results from different parts of the experiment will be presented, herein the surface elevation of the incident waves in chapter 3.1, surface development and maximum runup in chapter3.2, velocity profiles from the swash zone in chapter 3.3, and air bubble investigation in chapter 3.4. Finally, a discussion of the findings will be present in the last chapter 4.

2. Experimental set-up and formulation

2.1. The wave tank

Laboratory experiments of non-breaking to plunging breaking waves in the swash zone were conducted in a 25m long and 0.51m wide wave tank located at the Hydrodynamics Laboratory at the University of Oslo. Incident waves were generated in an equilibrium depth of 20.5cm by a piston type wave paddle using the method described in [6]. A PETG (Polyethylene Terephthalate Glycol-modified) beach with an inclination of 5.1° was placed in the wave tank with its toe 529.81cm from the start position of the wave paddle. Two coordinate systems were introduced, one parallel to the still water level (x', z'), and one parallel to the beach (x, z) (See Figure 1). The origin of both is at the equilibrium shoreline.

Nominally, the amplitude to depth ratios, $\alpha = A/H$, should equal (0.1,0.12,0.2,0.3,0.4,0.5). However, imperfection in the generation and frictional effects along the wave tank reduced the heights slightly such that $\alpha \approx A/H$. An acoustic wave gauge (ultra Banner U-Gage S18U, sample frequency of 200Hz) measured the wave height at the toe of the beach and the amplitudes were found to be $A/H = (0.09865, 0.1191, 0.1977, 0.2959, 0.3939, 0.4863)$

Sett inn rikti
amplitude som e
gitt av BIM

2.2. Instrumentation, measurements

To obtain velocity fields in the swash zone, images were captured at four different field of views (FOV), located upward along the beach (Table 1). The different FOV's are denoted with roman numbers. The water

Figure 1: *Sketch of the experimental set-up.*

FOV:	I	II	III	IV
Location, x:	[8.49 - 13.04]	[36.35 - 40.26]	[77.55 - 81.53]	[117.76 - 121.80]
Location, z:	[-0.05 - 3.78]	[-0.16 - 3.54]	[-0.04 - 3.79]	[-0.85 - 3.09]

Table 1: *Location of the different FOVs in cm. The dimensions of the FOVs are approximately 4cm x 4cm.*

in the tank was seeded with polymid particles with diameters of approximately 50 μm. A Quantronix Darwin Duo pulsed laser generated a light sheet parallel to the centreline of the wave tank, and a Photron SA5 high speed camera (1024 x 1024) synchronized with the laser, captured images of the illuminated particles. A Carl Zeiss Makro- Planer 2/50 zf lens was used. Images were collected at 3000 frames per seconds (fps). The image processing were performed in DigiFlow [3]. PIV was performed using interrogation windows of 32 x 8 pixels with a 75% overlap. Oblong interrogation windows are beneficial in boundary layer flow and have been employed previously in [7] and [8]. An averaging of 10 images was applied to reduce noise from the data. The number of images used in the average was carefully selected, so that the mean results were not affected by the averaging.

To investigate air bubbles encapsulated by the plunging breakers, the camera was moved further away from the wave tank, resulting in much larger FOV than the FOVs installed to obtain velocity fields. This FOV will be referred to as FOV A and is located at $x = [0-60]$cm. 500 fps were used in this investigation, and a continuous dedolight 400D was used as illumination, replacing the laser. A white background sheet was attached to the side wall of the wave tank and the water was dyed dark blue to increase the contrast in the images.

The maximum runup was measured by capturing images of the shoreline at its maximum position. A high speed Photron APX camera was mounted on rails above the beach in the wave tank with same inclination as the beach. A high pulsed white light was used as illumination. The field of views were based on estimates

3

of the runup height for each case. The camera captured 125 frames per second. The maximum shoreline profiles were tracked manually for each wave.

Each experiment was repeated at least three times. The scatter δ_i for some measured quantity, x_i, is then calculated as,

$$\delta_i = \frac{x_i - \overline{x}}{\overline{x}} \tag{1}$$

where $\overline{x}$ is the mean over the repetitions and

To find a measure for irregularities of the velocities in the swash tongue, the standard deviation for the the three repepitions are calculated, at the differents FOV. Deviations are extracted at times where the mean flow in an area from z=(0 - 0.6)cm is [40, 0, 40]cm/s.

$$\sigma = \frac{1}{N} \sum \sqrt{(x_i - \overline{x})^2} \tag{2}$$

The average deviations are also calucuate from the area of z=(0 - 0.6)cm. Here M corresponds to number of gridpoints in z-direction in this area.

$$\overline{\sigma} = \frac{1}{M} \sum (\sigma_j) \quad j = 1..M \tag{3}$$

2.3. The potential flow and boundary layer models

The evolution of the waves during shoaling, as well as the runup for the smallest amplitude, were computed by a BIM (Boundary Integral Model) for fully nonlinear, inviscid flow. This model breaks down when a plunger re-attaches with fluid or impacts the beach. Moreover, the model becomes singular when the contact angle at the shoreline exeeds 90° and the results also become unreliable for contact angles slightly smaller.

The potential flow model also provides the outer flow and the pressure gradient which are used as input to a FDM viscous boundary layer model. However, the coupling between the models is only one way as there is no feed-back from the boundary layer to the potential flow model. More details on both models are given in [8].

The simulations temporal resolution for all the waves was 0.0073s for the smallest wave and the number of grid points is 600 and three runs were a refinement gives runup values with less than 1% difference. The same has

Grid refinement?

3. Results

Visual inspection of the experiments revealed that the cases with normalized amplitude $A/H = 0.0989$ and $A/H = 0.1191$ did not break until the draw-down, while all the other cases developed into plunging breakers at or before the equilibrium shoreline. The plunger breakers encapsulated large amounts of air, which resulted in air bubbles in the swash tongue of the breaking waves (Figure 2).
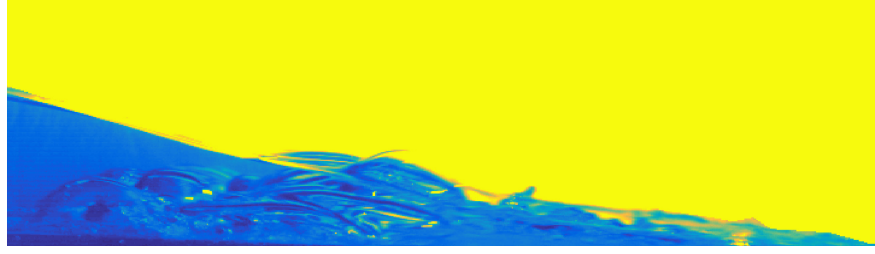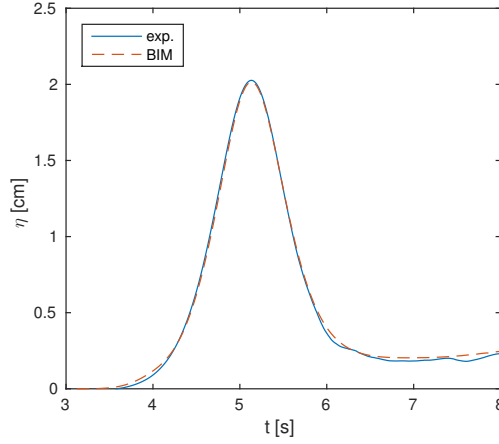
4

Figure 2: *Image of the swash tongue for $A/H = 0.4874$.*

Figure 3: *Measured and computed surface elevation for $A/H = 0.0989$.*

3.1. Surface elevation of the incident waves

The amplitude of the smallest amplitude wave is determined by a simple correction scheme. First the maximum of the series from the acoustic gauge is used as solitary wave amplitude in the BIM model. For the lowest wave this value is $\eta_m/H = ...$ When BIM data are extracted at the gauge position we then obtain a slightly too large surface elevation, due to the reflection from the beach, namely $\eta_b/H = ...$ We then adjust the amplitude according to $A = \eta_m - (\eta_b - \eta_m)$. The result is $A/H = 0.0989$ and the comparison with BIM results, obtained with this amplitude for the incident wave, is shown in Figure 3. When the surface elevation of the incident waves are very steep, the ultra sonic signal will not get reflected back to the sensor. This leads to dropouts in the measurements, which have been filled in by linear interpolation. Cubic polynomial regression is used to remove noise from the signal. The surface elevation measurements are in agreement with computed surface elevation from the BIM simulatitions.

3.2. Surface development and maximum runup

To investigate shoaling and runup of the waves both simulation and measurements have been conducted. BIM simulations of the near-shore evolution model is shown in figure 4). For reasons explained previously we only compute the runup for the smallest wave $A/H = 0.0989$. The computed time, inundation length and height for maximum runup were $t = 9.08$s, $r = 114.82$cm (measured along the beach), and $R/A = 5.05$
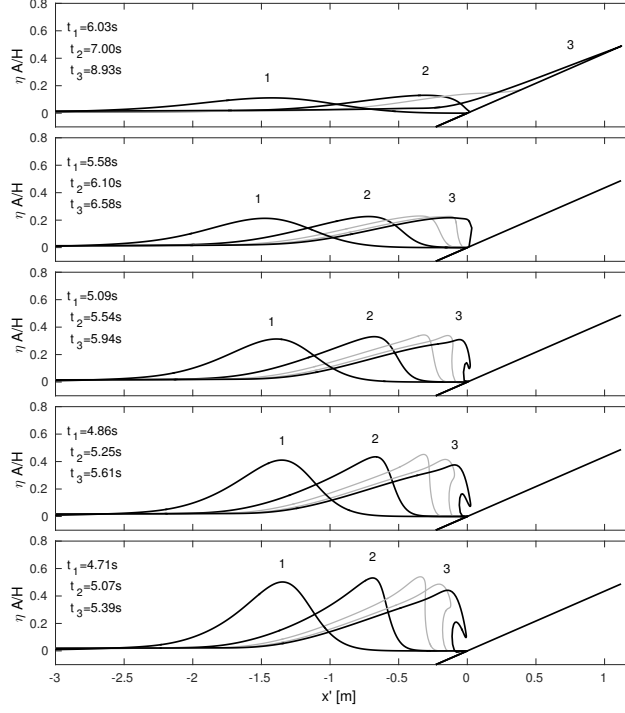
5

Figure 4: *BIM simulation of the waves the upper to lower figures correspond to $A/H = (0.0989, 0.1981, 0.2958, 0.3939, 0.4874)$, respectively. In the top panel the curve marked 3 corresponds to the time of maximum runup.*

respectively. The BIM model had some difficulties with the waves with amplitude $A/H = 0.1191$. For the other cases shown the numerical model describes the evolution of the plunger, but nothing beyonds its impact onshore.

The measured maximum runup heights and deviations for each waves are available in Table 3. Compared to the teoretical values above, for $A/H = 0.0989$, the maximum runup height is reduced by 32% and the maximum occurs 0.22s later. The BIM model does not account for viscous effect or surface tension, and this is the likely reason for the differences. [8] reported differences that were similar, but were smaller in magnitude due to a steeper slope angle of $10.54°$ which leads to thicker flow depths and shorter inundation. In fact, in figure 5 we observe transverse variations in the experiments and the average run up height is more than 5% smaller than the maximum one. The table shows that the maximum runup is repeatable for all waves including the breaking ones.

The shoreline at maximum runup are shown in Figure 5.It is fairly repeatable for the amplitue close to 0.1 times the depth (Figure 5a), but has a wedge-like shape. This is presumably due to a cross-wise deformation of the beach which has been measured using a straightedge and a feeling gauge. The typical maximum suppression in each transect of the beach was 3mm. If we assume that the depressions were unsystematic and that the later stages of runup are governed by gravity alone (see, for instance, [6]) this should correspond to a variation of 3cm on a 1 in 10 slope beach. However, even though the flow depth is small during runup, the momentum transport due to the pressure is still noticeable (inferred from the simulations, results not

Should hav
had the averag
runup height

6

A/H	$r[cm]$	R/A	$e_r[\%]$	t	$e_t[\%]$
0.0989	87.25	3.82	1.68	8.86 s	0.15
0.1191	105. 67	3.85	0.27	8.67 s	0.15
0.1981	147.37	3.22	0.93	8.53 s	0.31
0.2958	191.67	2.80	1.08	8.03 s	0.78
0.3938	227.42	2.50	0.11	7.82 s	0
0.4874	267.46	2.37	2.27	7.30 s	1.64

Table 2: *Maximum runup measurements where A/H is normalized amplitude, r is the runup in the direction along the beach, R is the vertical projection of the maximum runup, t is the time corresponding to max runup and e is the estimated error in the measurement*
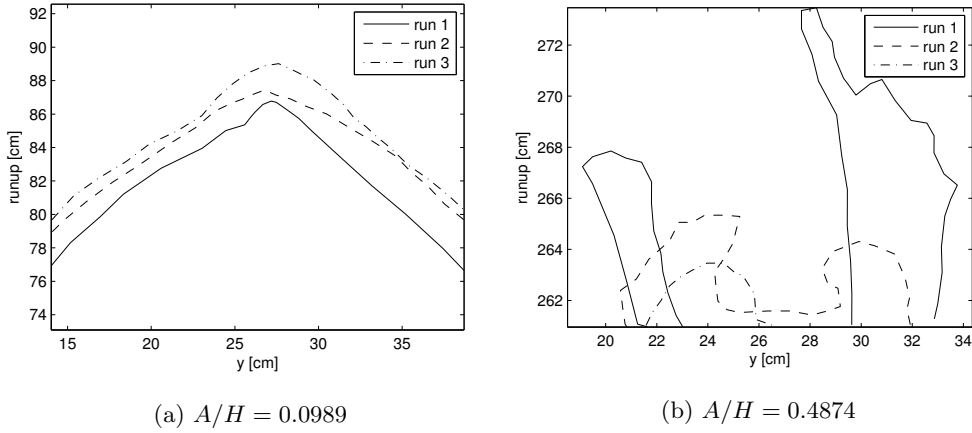

(a) $A/H = 0.0989$ (b) $A/H = 0.4874$

Figure 5: *Shoreline shapes at max runup.*

shown). More importantly, there is a systematic suppression at the center-line of the beach and the beach width is 50cm, which is comparable to the inundation length for the smallest amplitude. Hence, another relevant estimate of the runup variation is the suppression times the contact angle (angle of fluid wedge during runup) in radians. In the simulations this angle approaches $0.5°$ at maximum runup, which yields a a variation in x of 30cm. This is modified by the the capillary affects that affects the contact angle and shape of fluid body near the shoreline. Unfortunately, we cannot quantify this effect from the experiments. From Figure 5 it is clear that transverse variation is more in line with the latter estimate than the first one. The runup varies much more for the three repititions of the breaking wave $A/H = 0.4874$, resulting in irregularly shaped shorelines (Figure 5b).

An estimate of the arrival time of the wave for FOV II, III and IV, were measured based on the intensity changes in images captured at each FOV. Each image in each time series was compared to the initial image taken before the wave paddle starts. The image where the sum of light intensity differs more than a
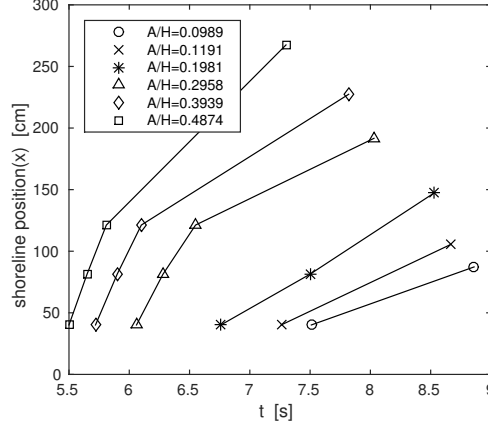
Figure 6: *Shoreline position as a function of time for all cases. The first measurements correspond to the swash tongue arrival time for FOV I, II, III. The last measuring point for all cases correspond to measurement of maximum runup*

$\overline{\sigma}\left[\frac{cm}{s}\right]$	$40\frac{cm}{s}$	$0\frac{cm}{s}$	$-40\frac{cm}{s}$
FOV I	0.52	0.24	0.51
FOV II	0.98	0.88	1.32
FOV III	1.97	0.88	1.48
FOV IV	2.82	1.35	1.45

Table 3: *Irregulariety for $\alpha = 0.50$, the men deviation from z=0-0.6 for the three repetitions*

given threshold (1000) from the initial image, correspond to the time when the wave enters that FOV. The measured shoreline positions as a function time are presented in Figure 6. The maximum error obtained for three different runs was 0.18%. This indicate that the shoreline motion was repeatable for each of the FOV.

3.3. Velocity profiles from the swash zone

Velocity profiles are extracted from the PIV data that are obtained from the four different FOV, approximately from 10cm to 120cm from the equilibrium shoreline. First, a comparison between computed BIM and measured PIV velocities for $A/H = 0.989$ will be given for FOV I and II, (See Figure 7). There is good agreement between measured and computed velocity profiles. The computed velocities are larger in the front of the wave for both the FOVs. This complies with corresponding results in [8] where the delay of the experimental wave was linked to cappilary effects, while an accumulative reduction of velocity, and hence runup height, was related to the viscous bodary layers at the beach. Hence, the BIM computation over-predicts the maximum runup as given in the previous section.   Values ???

FOV II is located approximately 40cm from the origin, and velocity profiles obtained from this FOV are shown in Figure 8. For $A/H = 0.1981$ the particle density was too sparse close to the surface, which led to
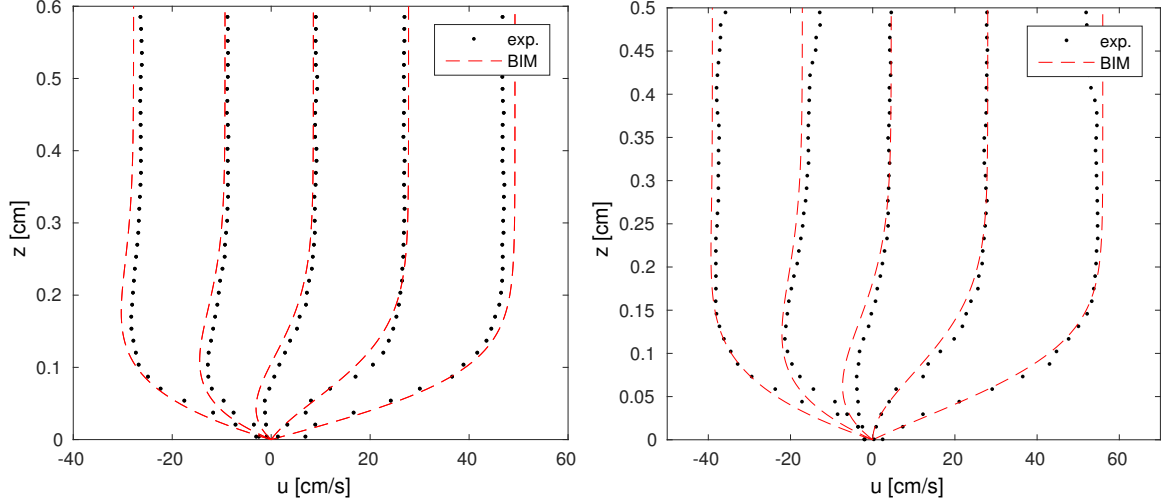
Figure 7:

Left: Velocity profiles from FOV I x=8.7cm t=[7.48, 7.82, 8.15, 8.48, 8.81]s

Right: Velocity profiles from FOV II x=40.1cm t=[7.76, 8.10, 8.76, 9.10]s

149 spurious vacillations in the velocity profiles near $z \approx 1$. Some distance below the surface a region of uniform
150 flow is apparent for all cases. Boundary layers are apparent for all the cases and they all display a flow
151 reversal prior to that of the outer flow. However, the evolution of the boundary layers for the amplitudes up
152 to just below $A/H = 0.2$ and those close to $A/H = 0.3$ and higher differ. The boundary layers for the higher
153 amplitudes appear more irregular with a thicker and less pronounced region of reversed flow in the boundary
154 layers. While the boundary layer for the lower amplitudes, including that of $A/H = 0.198$, appears laminar
155 the higher waves have boundary layers that presumably are in a transition to turbulence.

156 FOV III is located about 80cm from origo along the beach. For $A/H = 0.0989$ and $A/H = 0.1191$, the
157 swash tongues were too thin, and particles within the tongue were impossible to detect. Consequently, only
158 $A/H = 0.1981 - 0.4874$ will be presented for this FOV. None of the cases had an outer flow with constant
159 velocity at times close to outer flow reversal (Figure 9). This indicates that the motion was more irregular
160 for this FOV than for FOV II.

161 FOV IV is located about 120cm from where the still water reaches the beach. At this FOV, only
162 $A/H = 0.2958 - 0.4874$ will be presented due to the thin swash tongue for the other waves. Velocity
163 profiles are given in Figure 10. The velocity was less repeatable at this location than for the other FOVs.
164 The velocity profiles were more irregular, especially for $A/H = 0.4874$, where the average velocity profile
165 obtained before flow reversal resembles the parbolic velocity profiles from fully developed turbulent channel
166 flow, as described in [13].

167 Inspection of movies of the front of the swash tongue from FOV IV (furthest up the beach) shows that
168 a systematic swirling effect were present in the front of the swash tongue. Particle Tracking Velocimetry
169 (PTV) have been utilized to investigate this phenomenon. Figure 11 shows how the velocities vary at a

Geir: I really
cannot see
the evolution
of boundary
layer thick-
nesses. The
comparison
with Stoke
problem is
only relevant
for the stage
well before
flow reversal
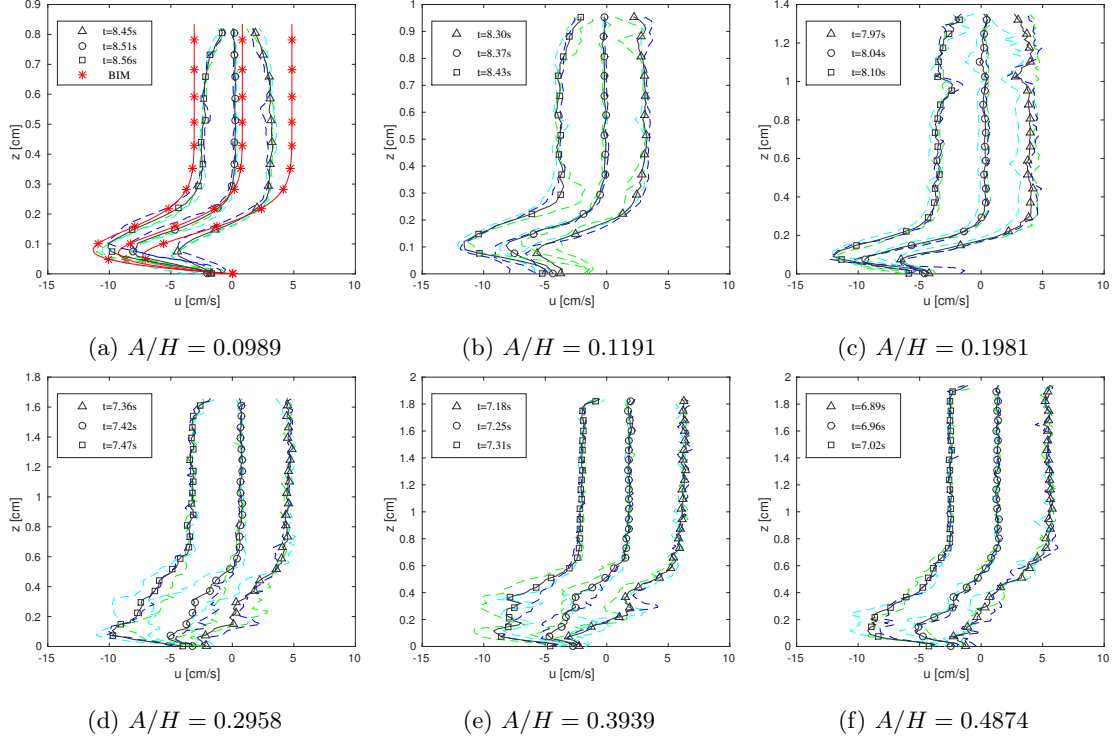Fig 11: is t=6.1
close to first ar-
rival of wave in
FOV III ?

9

Figure 8: *FOV II, mean velocity profiles before and after the outer flow reverses (△,◯,□). Colors: blue, cyan, green and red correspond to run 1,2,3 and BIM respectively. x = 40.11cm.*
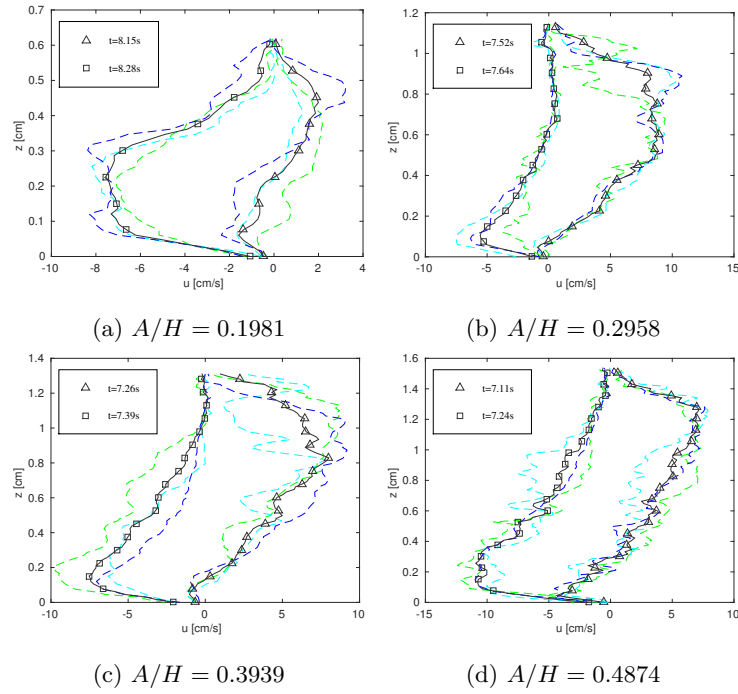

Figure 9: *FOV III, mean velocity profiles before and after the outer flow reverses (△,□). Colors: blue, cyan and green correspond to run 1,2 and 3. x = 81.40cm*

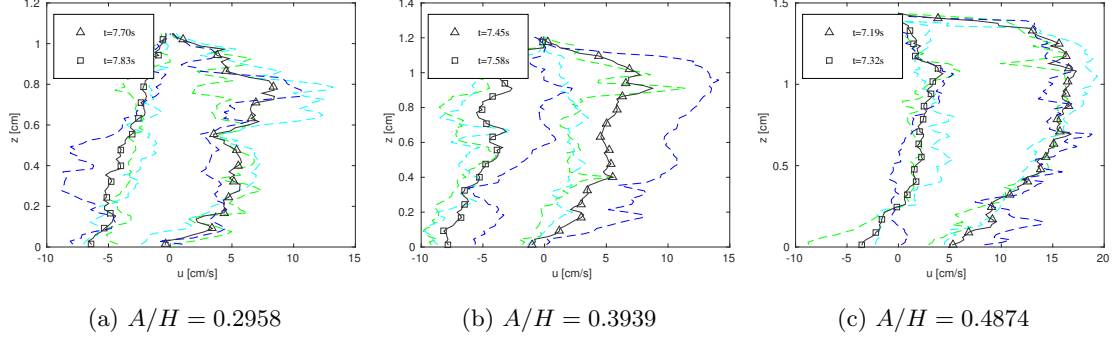(a) $A/H = 0.2958$ (b) $A/H = 0.3939$ (c) $A/H = 0.4874$

Figure 10: *FOV IV, mean velocity profiles before and after the outer flow reverses ($\triangle$,$\square$). Colors: blue, cyan and green correspond to run 1,2 and 3. $x = 121.25cm$*
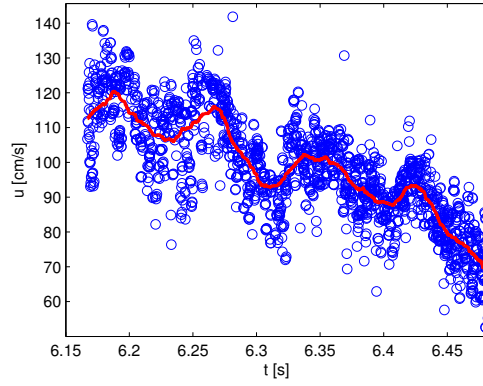

Figure 11: *FOV IV Collection of velocities of particles within a distance of 0.05cm from the point(x,z)=(120,0.3)cm. The data is collected from $A/H = 0.4874$, run 2. Blue circles: Raw data points. Red line: 2 order interpolation with 40 evaluation points*
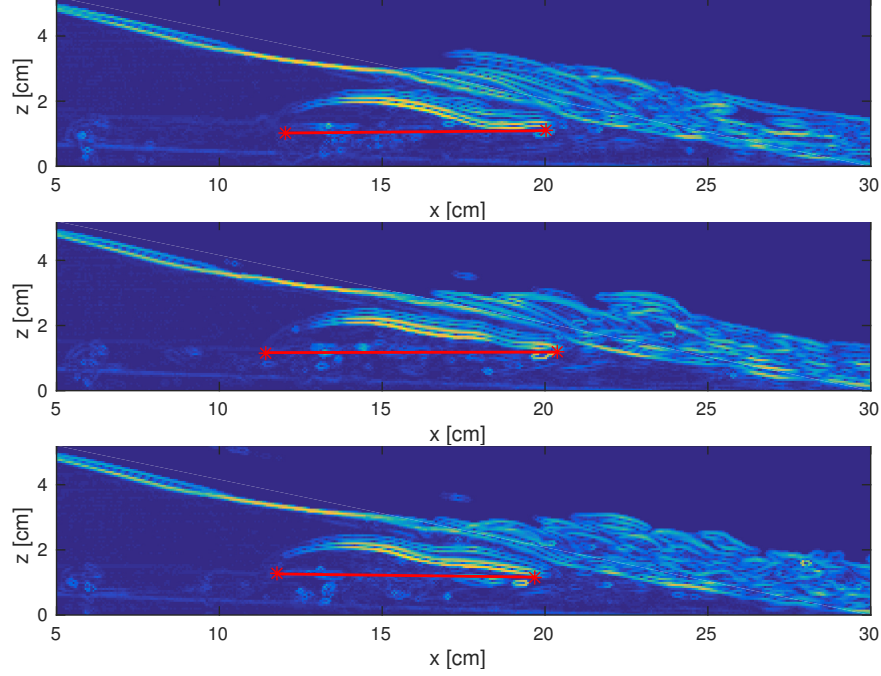
Figure 12: *A/H = 0.2958, run 1,2 and 3. t=6.06s*

single point in the fluid as a function of time. Superimposed a steady deceleration of the fluid there is an

oscillation. Flow in decelerating boundary layers are prone to instabilites. However, the oscillations do not

increase in magnitude and are present from the beginning. This indicates that the wave breaking induces

irregularities, possibly in the form of vortices, that prevails during the subsequent motion.

3.4. Bubble investigation

For the plunging breakers (*A/H* = ...) one large air bubble is encapsulated. As the waves propagated

upward the beach, this bubble disintegrates into smaller and smaller bubbles. Before maximum runup, all

the bubbles have escaped the surface. The images captured with the large FOV A provides some information

about this air bubble formation, (see Figure 12 and 13). To enhance the shape of the bubbles the gradient

magnitude image is represented. The shape of main bubble is oval with a thin tongue in the front, for

A/H = 0.2958. The shape of the main air bubble appears less repeatable for *A/H* = 0.4874. In particular,

in run 2 the large air bubble cannot be identified in the image at all. The length of the main bubble for three

different runs is given in Table 4. It is clear that images from the three different runs for *A/H* = 0.2958 is

more similar than for *A/H* = 0.4874.

The air bubble velocity in the direction along the beach is given in Table 5. The largest velocities were

obtained in the front of the bubbles, and may explain the shape of the thin tongue in the front of the air

bubble observed for *A/H* = 0.2958. The bubble findings indicates that the motion becomes more irregular

as the amplitude of the waves increases.
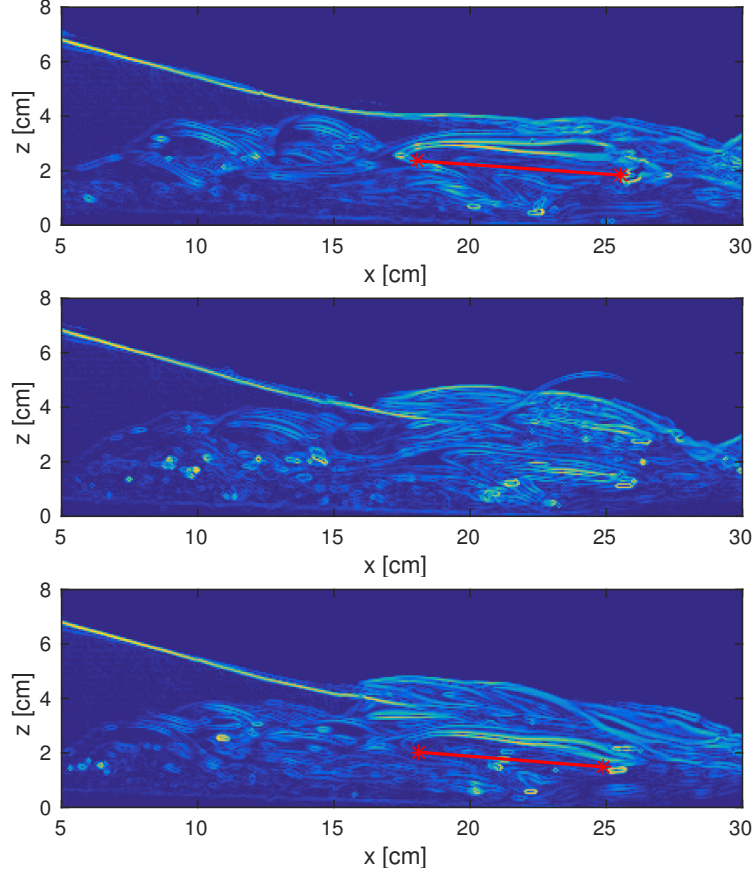
How the data is
obtained must b
better explained

12

Figure 13: $A/H = 0.4874$, run 1,2 and 3. $t=5.54s$

Main bubble size	Run 1 [cm]	Run 2 [cm]	Run 3 [cm]
$A/H = 0.2958$:	8.00	8.94	7.90
$A/H = 0.4874$:	9.24		8.17

Table 4: *Size of the main bubble measured at t=6.06s for case 30, and t=5.54s for case 50*

$A/H = 0.2958$	Run 1	Run 2	Run 3
Front velocity [m/s]	2.05	2.20	2.48
Tail velocity [m/s]	2.10	2.05	2.23
$A/H = 0.4874$			
Front velocity [m/s]	3.26		2.01
Tail velocity [m/s]	1.58		2.23

Table 5: *Velocities along the beach for the main air bubble. t=6.06s for case 30, and t=5.54s for case 50*

4. Discussion

For runup of non-beaking solitary waves on a 5.1° slope we observe laminar boundary layers. The presumption of laminarity is supported by the good agreement found with boundary layers computed by combining a potential flow model with a standard boundary layer model on the beach. However, in accordance with [8] the potential flow model, without any feed back from the boundary layer model, overpredicts the maximum runup height by 30%. The discrepancies between computations and measurements, which is mainly be due to viscosity and capillary effects , are in reality larger since tiny deformation of the beach increases the maximum runup height in the experiments..

The measurement of the breaking waves showed that the fluid motion becomes more irregular and less repeatable as we move further up the beach. In addition, the motion was more irregular for the waves with the stronger plunger breakers than for those with smaller amplitude. The maximum runup was fairly repeatable, but marked an irregular transverse variations were observed for the breaking waves. The bubble investigation indicated that the air bubble shapes were repeatable for the waves with amplitude $A/H = 0.2958$ but not for waves with amplitude $A/H = 48.74$. Overall, irregular motion increases with larger breaking waves and as the waves propagate upwards the beach.

[1] Barnes, M. P., O'Donoghue, T., Alsina, J. and Baldock, T. [2009], "Direct bed shear stress measurement in bore-driven swash", *Coastal Engineering* .

[2] Cowen, E. A., A.M.ASCE, Sou, I. M., A.M.ASCE, Liu, P. L.-F., F.ASCE and Raubenheimer, B. [2003], "Particle image velocimetry measurements within a laboratory-generated swash zone", *J. Eng. Mech* .

[3] Dalziel, S. B. [2006], 'Digiflow user guide', `http://www.damtp.cam.ac.uk/lab/digiflow/digiflow.pdf`. [Online; accessed 20-Aug-2014].

[4] Elfrink, B. and Baldock, T. [2002], "Hydrodynamics and sediment transport in the swash zone: a review and perspectives", *Coastal Engineering* , Vol. 45, Elsevier, pp. 149–167.

[5] Grilli, S., Svendsen, I. and Subramanya, R. [1997], "Breaking criterion and characteristics for solitary waves on slopes", *Journal of waterway, port, coastal, and ocean engineering* , Vol. 123, American Society of Civil Engineers, pp. 102–112.

[6] Jensen, A., Pedersen, G. K. and Wood, D. J. [2003], "An experimental study of wave run-up at a steep beach", *Journal of Fluid Mechanics* , Vol. 486, Cambridge Univ Press, pp. 161–188.

[7] Liu, P. L.-F., Park, Y. S. and Cowen, E. A. [2007], "Boundary layer flow and bed shear stress under a solitary wave", *Journal of Fluid Mechanics* , Vol. 574, Cambridge Univ Press, pp. 449–463.

[8] Pedersen, G., Lindstrøm, E., Bertelsen, A., Jensen, A., Laskovski, D. and Sælevik, G. [2013], "Runup and boundary layers on sloping beaches", *Physics of Fluids (1994-present)* , Vol. 25, AIP Publishing, p. 012102.

[9] Peregrine, D. H. [1983], "Breaking waves on beaches", *Annual Review of Fluid Mechanics* , Vol. 15, Annual Reviews 4139 El Camino Way, PO Box 10139, Palo Alto, CA 94303-0139, USA, pp. 149–178.

[10] Petti, M. and Longo, S. [2001], "Turbulence experiments in the swash zone", *Coastal Engineering* .

[11] Pujara, N., Liu, P. L.-F. and Yeh, H. H. [2015], "An experimental study of the interaction of two successive solitary waves in the swash: A strongly interacting case and a weakly interacting case", *Coastal Engineering* , Vol. 105, Elsevier, pp. 66–74.

[12] Rivillas-Ospina, G., Pedrozo-Acuña, A., Silva, R., Torres-Freyermuth, A. and Gutierrez, C. [2012], "Estimation of the velocity field induced by plunging breakers in the surf and swash zones", *Experiments in fluids* , Vol. 52, Springer, pp. 53–68.

[13] White, F. M. and Corfield, I. [2006], *Viscous fluid flow*, Vol. 3, McGraw-Hill New York.